The Space Congress® Proceedings

1998 (35th) Horizons Unlimited

Apr 29th, 8:00 AM

Paper Session II-B - The Advanced Camera for the Hubble Space Telescope

Holland Ford
ACS Science and Engineering Instrument Definition Team

Frank Bartko
ACS Science and Engineering Instrument Definition Team

Pierre Bely
ACS Science and Engineering Instrument Definition Team

Thomas Broadhurst
ACS Science and Engineering Instrument Definition Team

Christ Burrows
ACS Science and Engineering Instrument Definition Team

Presenter Information

Holland Ford, Frank Bartko, Pierre Bely, Thomas Broadhurst, Christ Burrows, Edward Cheng, Mark Clampin, Jim Crocker, Paul Feldman, David Golimowski, George Hartig, Garth Illingsworth, Randy Kimble, Michael Lesser, George Miley, Susan Neff, Marc Postman, Marc Rafal, William Sparks, Zlatan Tsvetanov, Rick White, Pamela Sullivan, Carolyn Krebs, Douglas Leviton, Tom Lajeunesse, Bill Burmester, Sheri Fike, Rich Johnson, Bob Slusher, Paul Volmer, and Bob Woodruff

The Advanced Camera for the Hubble Space Telescope

Holland Ford[1], Frank Bartko[1], Pierre Bely[1], Thomas Broadhurst[1], Chris Burrows[1], Edward Cheng[1], Mark Clampin[1], Jim Crocker[1], Paul Feldman[1], David Golimowski[1], George Hartig[1], Garth Illingworth[1], Randy Kimble[1], Michael Lesser[1], George Miley[1], Susan Neff[1], Marc Postman[1], Marc Rafal[1], William Sparks[1], Zlatan Tsvetanov[1], and Rick White[1]; Pamela Sullivan[2], Carolyn Krebs[2], and Douglas Leviton[2]; Tom Lajeunesse[3], Bill Burmester[3], Sheri Fike[3], Rich Johnson[3], Bob Slusher[3], Paul Volmer[3], and Bob Woodruff[3]

1. ACS Science and Engineering Instrument Definition Team
2. Goddard Space Flight Center Management and Engineering Team
3. Ball Aerospace Management and Engineering Team

1. Instrument Overview

The Hubble Space Telescope (HST) *Advanced Camera for Surveys* (ACS) will have a high throughput, wide field, optical and I-band camera (WFC), a critically sampled high resolution camera (HRC), and a high throughput, moderate field of view far ultraviolet, solar-blind camera (SBC). The key characteristics of the ACS are listed in Table 1. The throughputs include the geometrical, scattering, and reflectivity losses from the HST optical telescope assembly (Burrows, HST OTA Handbook). Two figures are listed for the ACS efficiencies. The first is the efficiency using the quantum efficiency (QE) of the Scientific Imaging Technologies (SITe) 2K x 4K WFC CCDs and the SITe HRC 1K × 1K CCDs selected for the first build of the flight cameras. The second and higher efficiencies are those achieved with SITe CCDs processed and anti-reflection coated at Steward Observatory by Dr. Michael Lesser. We plan to use these better CCDs for the second build of the flight cameras.

Table 1: Key Characteristics of the Advanced Camera for Surveys

	WFC		HRC		SBC	
Prioritized Features	ACS WFC	WFPC2 f/12.9	ACS HRC	WFPC2 f/17.9	ACS SBC	FOC+COSTAR f/151
Max.Through-put (%@λnm)	36/49@600 nm	14.5@600 nm	24/25@600 nm	14@600 nm	6.1@121.6 nm	1.6@**150 nm
at 800 nm	29/36	7	17/17	7.0	6.1@121.6	0.81@121.6
at 400 nm	22/24	5.3	17/23	5.3	5.3@130	1.3@130
at 250 nm	---	3.0	11/23	3.0	4.1@140	1.4@140
					2.9@150	1.6@150
					1.7@160	1.5@160
FOV	200"×204"	143"×143"	26"×29"	35"×35"	26"×29"	7"×7"
Sampling @ 500 nm	Half	Quarter	Full	Half	Half***	Full
Polarization from design & coating	<1%	~5%	<5%	~5%	<1%	<1%

*The FOC is not solar blind; **Maximum in the FUV; ***@295 nm

For comparison, Table 1 includes the two cameras that ACS supercedes, the WFPC2 (ref. the WFPC2 Handbook) and the FOC (ref. the FOC Handbook). The ACS will provide large gains in sensitivity and field of view compared to the WFPC2 and the FOC. The product of the QE and

the field of view (the discovery efficiency) is a measure of how efficiently a camera can be used for surveys. The near infrared bandpass centered on 800 nm is particularly important for surveys to find galaxies at high redshift. The ACS will have a discovery efficiency that is 8 to 10 times better than the WFPC2 in the I-band. The WFC will have twice the resolution of the WF2, and the HRC, which fully samples the HST point spread function at wavelengths $\lambda \geq 500$ nm, will have twice the resolution of the PC2 camera.

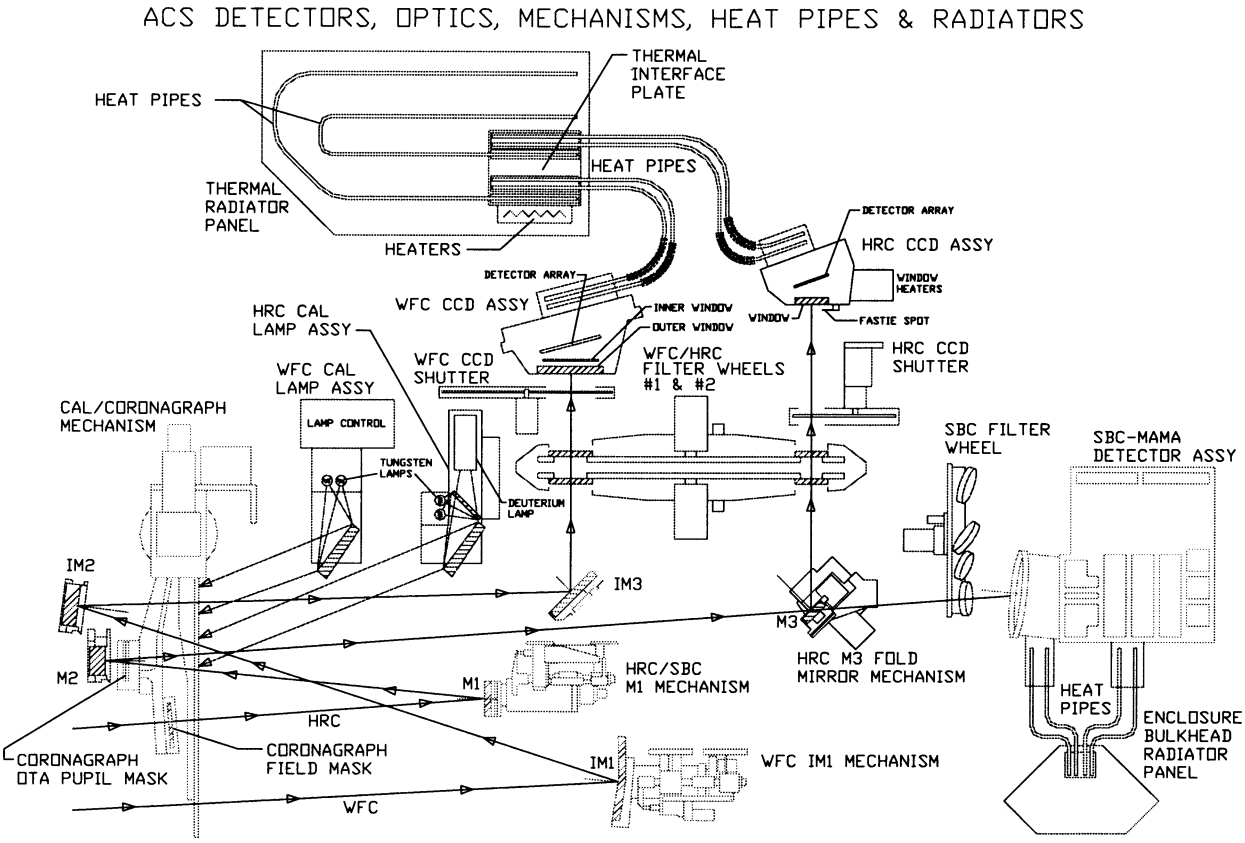

Figure 1 is a schematic of the ACS. The large WFC spherical mirror IM1 images the telescope pupil onto the small anamorphic asphere IM2. IM2, which is figured with the inverse spherical aberration in the HST primary, corrects the image and reimages the focal plane onto the WFC. IM3 corrects residual astigmatism in the image and reflects the light into the WFC. The three IM mirrors have a Denton over-coated silver coating for high reflectivity.

The HRC and SBC cameras share the M1 and M2 mirrors. The M3 flat either deflects the light into the HRC or allows unobstructed passage to the SBC. Because of the relatively low reflectivity of Al overcoated with MgF2, minimizing the number of reflections to the SBC helps improve its net efficiency.

The combined aperture door and calibration mirror insertion mechanism carries two opaque field stops for the coronagraph. Because of cost constraints, the stops are at the aberrated focus. A pupil mask is automatically positioned over the HRC M2 mirror when field stops are inserted into the beam. Exterior to the r = 0.9″ stop radius, the coronagraph will provide an order of magnitude better scattered light suppression than the WFPC2 camera.

The Swales Engineering heat pipes shown in Figure 1 connect to a metal thermal interface plate. This in turn is connected by heat pipes to a radiator panel on the ACS enclosure. The radiator panel radiates into the HST's aft shroud. The temperature within the aft shroud is gradually increasing because of increased power dissipation by HST replacement instruments and by the HST's slow loss of exterior reflectivity. Consequently, during ACS installation the astronauts will connect the interface plate to heat pipes that lead to an external radiator.

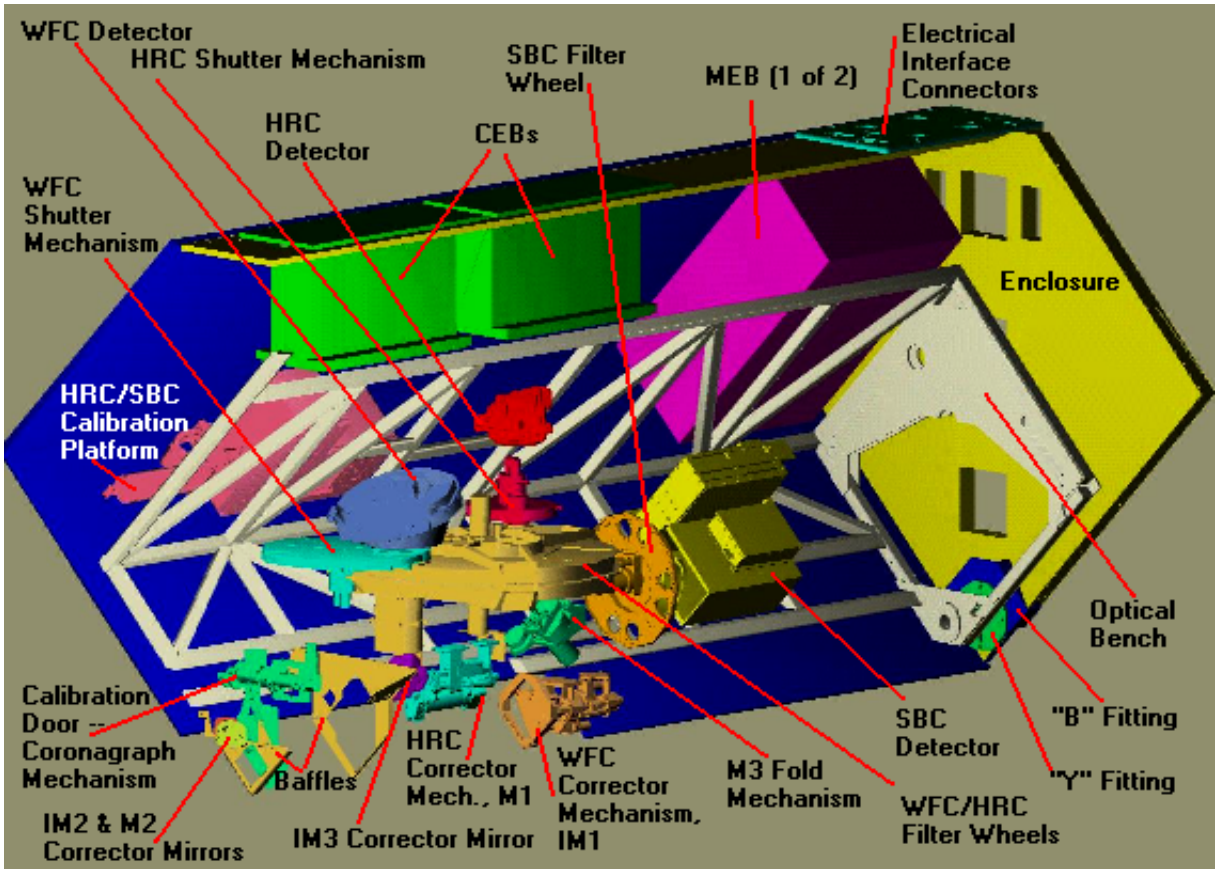

2. The Wide Field CCD Camera

The WFC has two 2K x 4K CCDs mounted side-by-side on a common aluminum nitride focal plane carrier. The biggest challenge in designing the WFC enclosure is to achieve an operating temperature of -80° C or colder while staying within the ACS power budget. This was accomplished by supporting the focal plane carrier on a single 4-stage Marlowe Theromoelectric Cooler (TEC). The 4K x 4K CCD is thermally isolated from the ACS by a double enclosure. The innermost enclosure and AR-coated fused silica window is mounted on four 2-stage TECs. The interiors of the two enclosures are gold plated to reduce thermal emissivity. The predicted temperatures of the inner enclosure for hot and cold operate are respectively -40° and -60° C. The entire enclosure is evacuated and sealed to avoid "gettering" by the cold CCDs of residual gases within the ACS and the HST. After the enclosure is sealed, four getters are fired within the enclosure to provide traps for residual gases from the CCDs and tape cables. Figure 3 shows a picture of the inner housing mounted on the large molybdenum baseplate which provides radiation protection for the CCDs. Figure 4 is a schematic that shows the CCDs within

the double enclosure. Passive heat pipes filled with ammonia attach to the bottom of the base-plate and “conduct” heat to the thermal interface plate (c.f. Fig. 1).

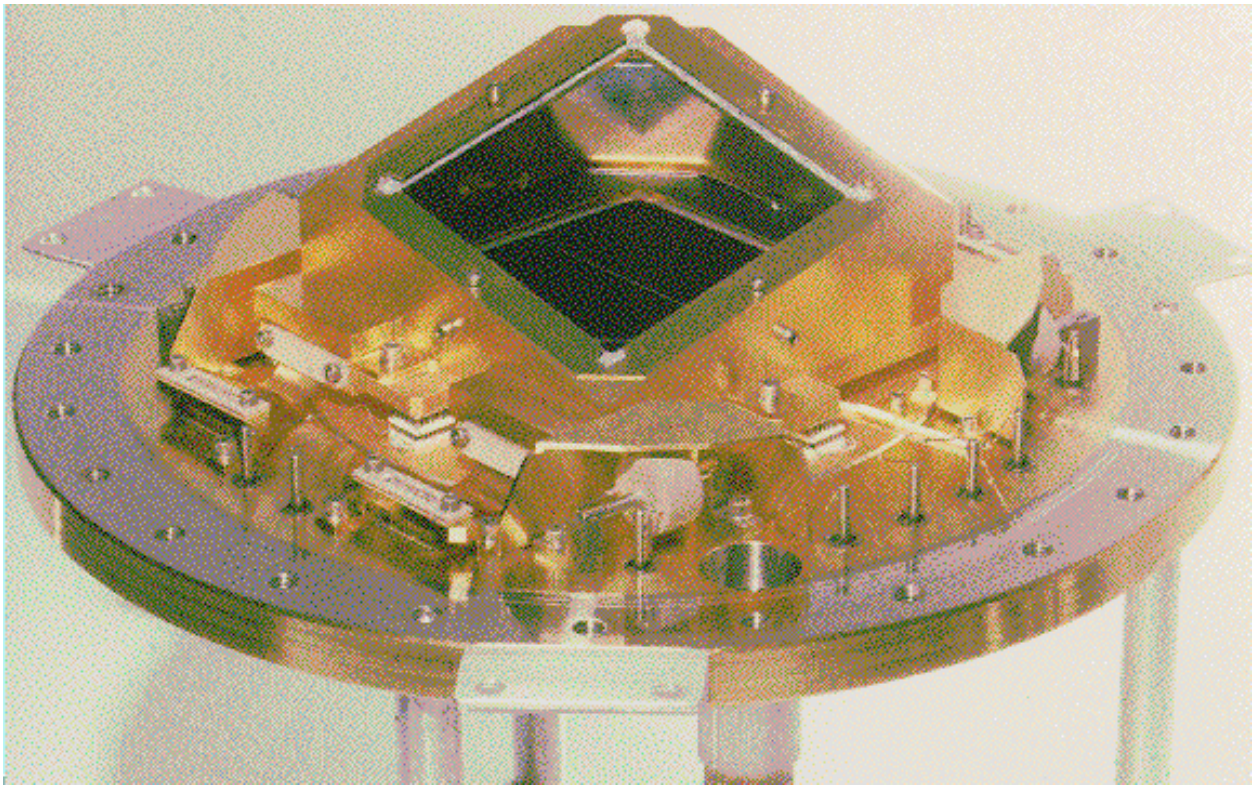

Figure 3. the two 2Kx4K CCDs can be seen through the window of the inner enclosure.

Figure 4. A schematic shows the WFC double enclosure mounted on the molybdenum baseplate.

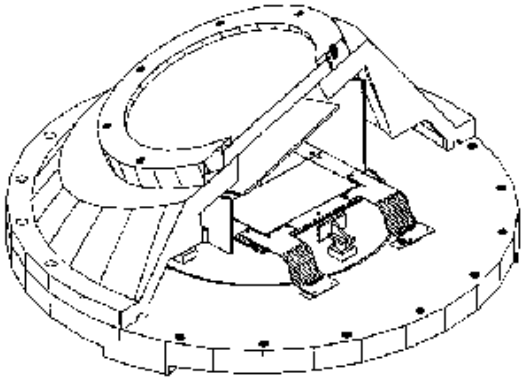

Quantum efficiency and rms read noise per pixel (rn) are usually the most important performance parameters in astronomy. The signal-to-noise ratio in deep, broad band, background-limited exposures is proportional to $(QE)^{0.5}$. In narrow band exposures the signal-to-noise will be proportional to $QE/(rn)^{0.5}$. The measured QEs for the Build 1 and 2 CCDs are shown in Figure 5. We expect the rms read noise of the four amplifiers to be ≤ 6 electrons when optimized and used with the flight electronics.

The amplifiers on the commercial SITe 2K x 4K CCD are positioned to allow abutment on three sides. This design gives 4096 parallel shifts and 2048 serial shifts during readout. Because exposure to cosmic rays slowly degrades the charge transfer efficiency (CTE), we used a cus-

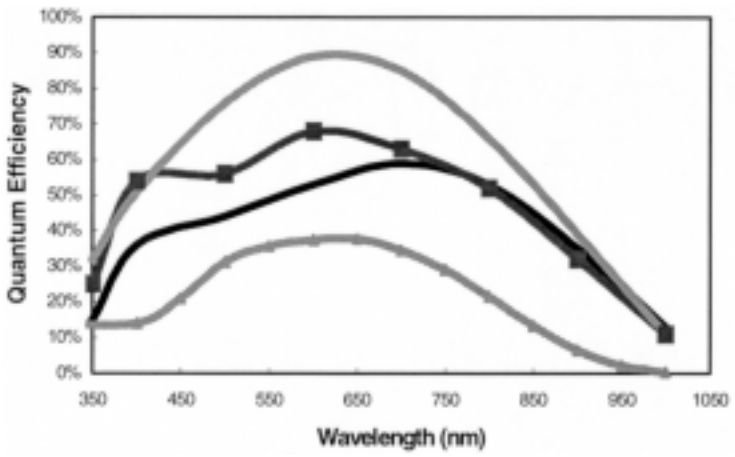

Figure 5. The quantum efficiencies for the Build 1 and 2 CCDs. The lowermost curve is the QE of the WFPC2 CCDs. The two middle curves are the Build 1 CCDs. The uppermost curve is the QE of a Build 2 CCD coated by Dr. Michael Lesser.

tom mask that enables us to simultaneously read the CCD through 2 amplifiers at opposite ends with 2048 parallel and 2048 serial shifts. The CTE of the Build 1 and Build 2 cameras will be ≥ 0.99998 at beginning of life. We expect the rms read noise to be better than 6 electrons per pixel, and the full well of the 15 micron square pixels to be ≥ 80,000 electrons.
The commercial SITe process bonds the CCD silicon wafer to a soda glass substrate. At wavelengths l ≥ 700 nm the silicon becomes progressively transparent, allowing light to pass into the translucent substrate and be scattered back into the silicon. At 900 nm as much as 30% of the detected light appears in a halo with a radius of tens of pixels. To prevent this halation, a layer of aluminum is now deposited on the frontside of the CCD before bonding to the glass substrate. The aluminum blocks the light and eliminates the halo out to l @ 950 nm.

3. The High Resolution Camera

The thermal enclosure and electronics for the HRC SITe 1K x 1K CCD camera are the same as the 1K x 1K CCD camera in the Space Telescope Imaging Spectrograph (STIS). The focal length of the camera was chosen to give an average plate scale of 0.025″ per 24 μ square pixel, thereby fully sampling the HST PSF at λ ≥ 500 nm. SITe has improved the UV response of their CCDs since delivering the STIS CCDs. Figure 6 shows the excellent enhanced UV QE of the CCD chosen for Build 1.

The CCD selected for Build 1 has a SITe coating with enhanced UV response, as shown in Figure 6. For comparison, we have included the QE of the STIS 1K x 1K CCD. This CCD has excellent cosmetics and readnoise, and excellent CTE. Table 2 summarizes the characteristics of the two CCDs.

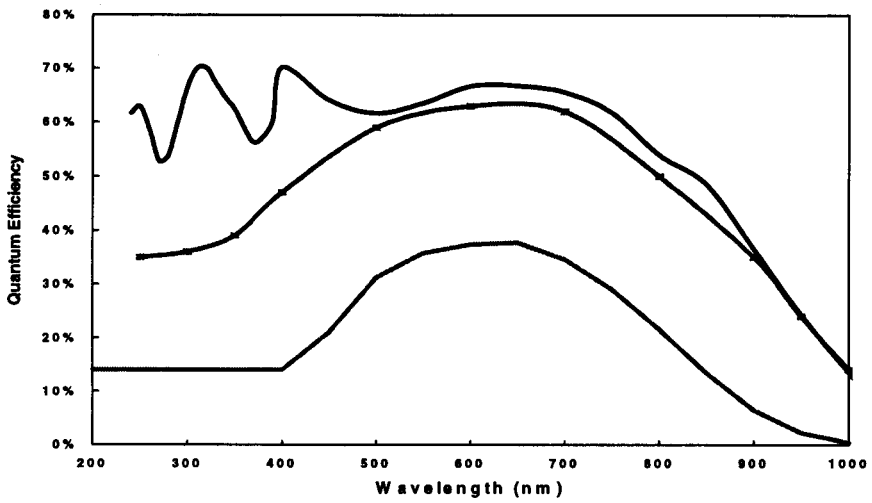

Figure 6. The top curve is the QE of the Build 2 HRC 1K x 1K CCD with Dr. Michael Lesser's UV-enhanced coating. The middle curve shows the QE of the SITe CCD with an enhanced UV response. The lowermost curve shows the QE of the WFPC2.

Table 2. Characteristics of the Flight HRC 1K x 1K CCDs		
Quantity	Build 1 CCD	Build 2 CCD
Gain @ 1620 e (μV/e)	1.70	1.23
Parallel CTE @ 1620 e	0.99998	0.999995
Serial CTE @ 1620 e	0.999998	0.999997
Avg. Read Noise (e)	4.1	5.4
Dark @ –80° C (e/pix/hour)	21	20

4. The Solar Blind Camera

The SBC is optimized for highest throughput at 121.6 nm (the wavelength of Lyman a in the hydrogen atom). The SBC uses a STIS flight spare photon counting array detector with an opaque CsI photocathode and a C-plate micro-channel plate. The 26″ x 29″ image is sampled at 0.030″/pixel. The resultant image quality at the photocathode surface is better than λ/15 everywhere in the FUV, and nearly uniform with field. The wavefront error varies from 0.025 to 0.064 waves rms at 143.5 nm over the field. The design is optimized from 121.6 to 160.8 nm. When operated monochromatically at different wavelengths within the CsI response, there is very little variation in the image. When operated broad band, some lateral color is evident in the image. For instance, the field weighted rms wavefront error in waves at 632.8 nm is 0.0111 for an operational wavelength of 143.5 nm, 0.0113 for 121.6 nm, 0.0114 for 160.8 nm, and 0.0161 nm when operated broadband.

The characteristics of the SBC, including the measured DQE at the ACS angle of incidence into the detector, are summarized in Table 3.

Table 3. Performance Characteristics of the SBC Detector			
Quantity	Value	Wavelength	DQE
Wavelength Range	112 nm – 119 nm	121.6	0.192
Spatial Resolution (FWHM)	28.2 microns	125.4	0.189
Dark Count @ 38° C (c/s/pix)	2.5×10^{-4} global	135.4	0.177
Dark Count @ 38° C (c/s/pix)	6.9×10^{-4} peak	140.3	0.154
Flat Field Uniformity	± 6.2 % rms (1σ)	148.7	0.125
Visible Light DQE		λ > 400 nm	$< 1.16 \times 10^{-9}$
Broken Electrodes	1		
Bright Spots > 1 c/s	2		
Dark Spots	3		
Spatial Non-Linearity	5 μ/mm (maximum)		
Local Dynamic Range	350 c/pix/s		
Global Dynamic Range	3.6×10^{5} c/s		

5. Filters for the Cameras

The ACS filters are listed in Table 4. A detailed discussion of the filters can be found in Ford et al. 1995. Several characteristics of the filters are worth noting. For photometric continuity between the WFPC2 and the ACS, we have included the three most frequently used WFPC2 broadband filters, F555W, F606W, and F814W. The bandpasses of our F658N, F502N, and F344N filters were tailored to allow Hα+[NII], [OIII]λ5007, and [NeV] WFC/HRC observations of galaxies from the local group out to a recessional velocity of 3000 km s^{-1}. Our 2% continuously variable bandpass filters will enable narrow bandpass observations of any emission lines between 370 nm and 1050 nm. The HRC UV filters F220W, F250W, and F350W have two to three times the in-band throughput of the equivalent WFPC2 filters. When combined with the approximately eight times higher sensitivity of the HRC Build 2 CCD, the sensitivity gain in the near UV will be 20 or more relative to the WFPC2. Finally, we have optical and near UV polarizing filters that can be combined with filters in the complementary wheel. Polarametric observations with the low scattering (silver coated mirrors) and high sensitivity WFC should be far more effective than polarimetric observations made with the WFPC2.

Table 4. Filter Description					
	Name	Central λ or range (nm)	FWHM	Descriptive Name	Allowed Config
Filter Wheel #1	F555W	534.6	119.3	Johnson V	WFC, HRC
	F775W	776.4	152.8	SDSS I	WFC, HRC
	F625W	631.8	144.2	SDSS r	WFC, HRC
	F658N	658.1	7.8	Hα	WFC, HRC
	F850LP	944.5	122.9	SDSS z	WFC, HRC
	POL0UV	250-700	*	UV Polarizer 0 Deg	WFC, HRC
	POL60UV	250-700	*	UV Polarizer 60 Deg	WFC, HRC
	POL120UV	250-700	*	UV Polarizer 120 Deg	WFC, HRC
	F892N	891.7	15.4	Methane	WFC, HRC

	F606W	590.7	234.2	Broad V	WFC, HRC
	F502N	502.2	5.7	OIII	WFC, HRC
	G800L	55-100	n/a	GRISM	WFC, HRC
	F550M	558	54.7	Narrow V	WFC, HRC
	F475W	476.0	145.8	SDSS g	WFC, HRC
Filter Wheel #2	F410W	402.3	73.2	WFC u	WFC, HRC
	F814W	833.3	251.1	Broad I	WFC, HRC
	FR388N	371-405	2%	OII Ramp (middle)	WFC, HRC
	FR423N	405-442	2%	OII Ramp (inner)	WFC
	FR462N	442-482	2%	OII Ramp (outer)	WFC
	F435W	429.7	103.8	Johnson B	WFC, HRC
	FR656N	627-685	2%	Hα Ramp (middle)	WFC, HRC
	FR716N	685-747	2%	Hα Ramp (inner)	WFC
	FR782N	747-816	2%	Hα Ramp (outer)	WFC
	POL0V	450-800	**	Visible Polarizer 0 Deg	WFC, HRC
	F330W	335.4	58.8	HRC u	HRC
	POL60V	450-800	**	Visible Polarizer 60 Deg	WFC, HRC
	F250W	269.6	54.9	Near-UV filter	HRC
	POL120V	450-800	**	Visible Polarizer 120 Deg	WFC, HRC
	PR200L	200-400	n/a	HRC PRISM	HRC
	F344N	343.4	6	NeV	HRC
	F220W	229	64.9	Near-UV filter	HRC
	FR853N	816-891	2%	IR Ramp (inner)	WFC
	FR931N	891-972	2%	IR Ramp (outer)	WFC
	FR1016N	972-1061	2%	IR Ramp (outer)	WFC
	FR459M	381-537	9%	Broad Ramp (middle)	WFC, HRC
	FR647M	537-757	9%	Broad Ramp (inner)	WFC
	FR914M	757-1071	9%	Broad Ramp (middle)	WFC, HRC
	FR505N	482-527	2%	OIII Ramp (middle)	WFC, HRC
	FR551N	527-575	2%	OIII Ramp (inner)	WFC
	FR601N	575-627	2%	OIII Ramp (outer)	WFC
Filter Wheel #3	F165LP	165-180	n/a	Suprasil	SBC
	F150LP	150-180	n/a	Crystal Quartz	SBC
	F140LP	140-180	n/a	BaF_2	SBC
	F125LP	125-180	n/a	CaF_2	SBC
	F122M	122	9%	Ly-α	SBC
	F115LP	115-180	n/a	MgF_2	SBC
	PR130L	130-180	n/a	CaF_2 PRISM	SBC
	PR110L	110-180	n/a	LiF_2 PRISM	SBC

* Used in combination with filters in Filter Wheel 2 covering this wavelength range.
**Used in combination with filters in Filter Wheel 1 covering this wavelength range.

6. References

Biretta. J.A. et al. 1996, WFPC2 Instrument Handbook, Version 4 (Baltimore: STScI).

Burrows, C. 1990. OTA Handbook, Version 1 (Baltimore: STScI).

Ford, H.C. et al. 1996, "The Advanced Camera for the Hubble Space Telescope," in Space Telescopes and Instruments IV, Proc. SPIE, Vol. 2087 (Bellingham, WA: SPIE), 184.

Nota, A. et al. 1996, FOC Instrument Handbook, Version 7 (Baltimore: STScI).